ACS APPLIED MATERIALS & INTERFACES

Letter

www.acsami.org

Novel Highly Active Visible-Light-Induced Photocatalysts Based on BiOBr with Ti Doping and Ag Decorating

Guohua Jiang,*[,†,‡] Rijing Wang,[†,‡] Xiaohong Wang,[†,‡] Xiaoguang Xi,[†,‡] Ruanbing Hu,[†,‡] Yang Zhou,[‡] Sheng Wang,[†,‡] Tao Wang,[†,‡] and Wenxing Chen[†,‡]

[†]Key Laboratory of Advanced Textile Materials and Manufacturing Technology (ATMT), Ministry of Education, [‡]Department of Materials Engineering, College of Materials and Textile, Zhejiang Sci-Tech University, Hangzhou 310018, P. R. China

Supporting Information

ABSTRACT: Visible-light-induced BiOBr photocatalysts with Ti doping and Ag decorating were prepared by three methods (chemical reduction, photoreduction, and thermal reduction). Compared to the tannin acid reduction and photoreduction, the solvothermal reduction method was relatively simple and efficient, and Ag doping and loading simultaneously occurred. The as-prepared 3% Ag/Ti-dope BiOBr photocatalysts exhibited the flowerlike microsphere structures that assembled by nanoplates, and showed higher photocatalytic activity and excellent durability.

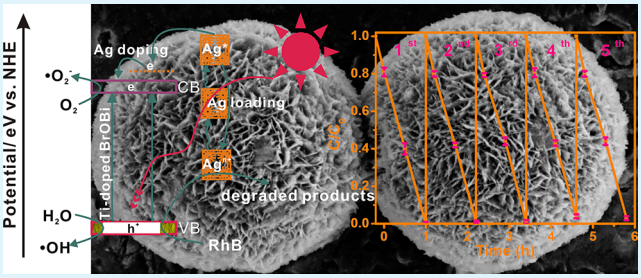

KEYWORDS: *solvothermal reduction, Ti-doped BiOBr, Ag decorating, flower-like microsphere, photocatalysis*

Since the discovery of their photocatalytic activity under UV- or visible-light illumination, bismuth oxyhalides have been extensively studied because of their potential application in degradation of organic pollutants.[1−3] Especially of BiOBr, crystallizing in a layered structure composed of $[Bi_2O_2]^{2+}$ layers which were interleaved with double Br layers, has attracted considerable attention because of its suitable band gap, stability and relatively superior visible-light-induced photocatalytic activity.[4−6] However, BiOBr photocatalysts still cannot meet the requirements of practical application attributing to their insufficient photodegradation ability. Therefore, it is promising and indispensable to enhance their photocatalytic efficiency by modification, such as doping, coupling and supporting, etc.[7−10] In recent years, there has been increasing interest in noble metal decorated photocatalytic materials, because noble metal (Ag, Au, Pt, etc.) nanoparticles exhibit strong absorption of light in the UV−vis region resulted from their surface plasmon resonance (SPR) property or act as the electron receptor.[11−13] When anchoring noble metal nanoparticles on the light-excited semiconductors, they can effectively enhance photocatalyitc activity via the improvement of photoabsorption and interfacial charge transfer.[14−17] In addition, the doping could enhance the photocatalyst's degradation ability due to the improvement of the charge separation.[18−21] Moreover, decorating contents, distribution, and mode (loading or doping) of noble metal are key parameters for improving the photocatalyst's activity. Potentially, functionalizing BiOBr with Ti and Ag, which combines the microsphere structure of BiOBr and the unique catalytic property of Ag and Ti, will help to find novel properties or enlarge the application of BiOBr materials.

In this letter, toward investigating the noble metal decorating, three methods (chemical reduction, photoreduction, and thermal reduction) were applied to prepare Ag/Ti-doped BiOBr based on our preliminary research of Ti-doped BiOBr photocatalysts (Experimental section in the Supporting Information).[22] Tannin acid simultaneously serves as a reducing agent and stabilizing agent to produce Ag nanoparticles dispersed on flower-like structure of Ti-doped BiOBr (C−Ag), Ag/Ti-doped BiOBr can also be obtained under UV irradiation (P−Ag). Most importantly, a facile solvothermal approach was applied to directly prepare Ag/Ti-doped BiOBr composites (T−Ag) with different concentration of Ag (1%, 3%, and 5%, relative to the final samples). The resulting composites manifest excellent photocatalytic activity on the degradation of Rhodamine B (RhB).

The morphologies and structures of C−Ag, P−Ag, and T−Ag were first characterized by field-emission scanning electron microscopy (FE-SEM) and high-resolution transmission electron microscopy (HR-TEM). Figure 1a shows a low-magnification FE-SEM image of an individual flower-like microsphere of Ti-doped BiOBr sample. After the chemical reduction of tannin acid, a large amount of Ag nanoparticles deposited on the surface of Ti-doped BiOBr microsphere (Figure 1b). Figure 1c exhibits the mondisperse Ag nanoparticles can also be found on the surface of Ti-doped BiOBr microsphere through photoreduction, which is in accordance with the TEM images (Figure S1 in the Supporting Information). Above all, these results indicate that C−Ag and P−Ag photocatalysts were successfully prepared. And a facile solvothermal method was used to prepare T−Ag composites.

Received: July 1, 2012
Accepted: August 22, 2012
Published: August 22, 2012

   dx.doi.org/10.1021/am301177k | ACS Appl. Mater. Interfaces 2012, 4, 4440−4444

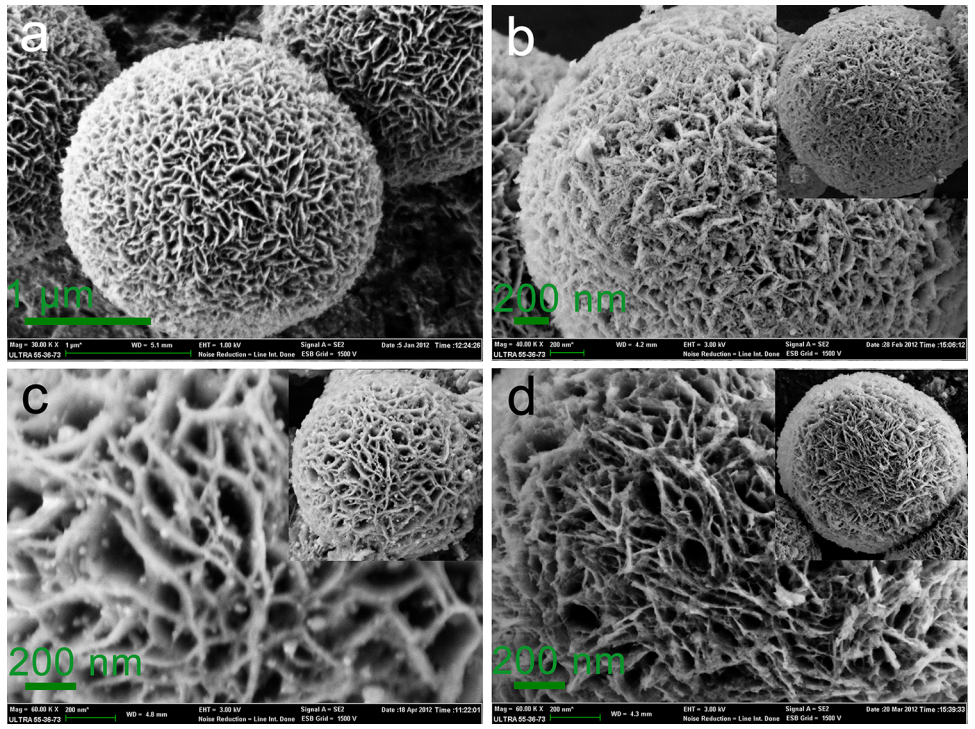

Figure 1. FE-SEM images of (a) the as-prepared Ti-doped BiOBr microsphere, (b) C−Ag, (c) P−Ag, and (d) T−3% Ag.

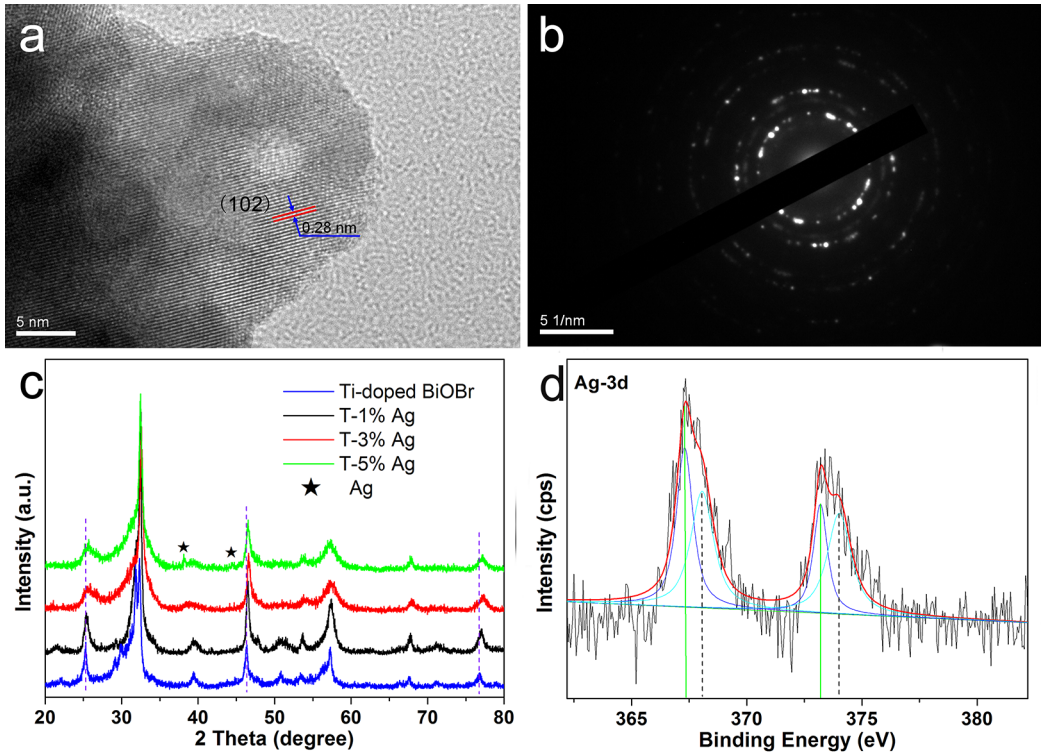

Figure 2. (a) HR-TEM image and (b) SAED pattern of T−3% Ag composites, (c) XRD patterns of Ti-doped BiOBr and T−Ag samples, and (d) XPS spectrum of T−3% Ag composites.

Figure 1d presents the FE-SEM image of T−3% Ag, the surface morphology of the T−3% Ag did not appear to be meaningfully different from that of Ti-doped BiOBr samples, which indicates the structure of microsphere can be obtained after the introduction of Ag and Ti. In addition, Ag contents have little effect on the surface morphology of the final samples (Figure S2 in the Supporting Information). The HR-TEM image of T−3% Ag in Figure 2a shows a well-defined crystallinity of BiOBr with a lattice spacing of 0.28 nm, which is assigned to the (102) plane of tetragonal phase. The corresponding selected area electron diffraction (SAED) pattern (Figure 2b) reveals that the sample has the polycrystalline nature of T−3% Ag.

dx.doi.org/10.1021/am301177k | ACS Appl. Mater. Interfaces 2012, 4, 4440−4444

Ti doping and Ag decorating were simultaneously achieved by a facile solvothermal method, which were confirmed by XRD, EDS and XPS results. As shown in Figure 2c, all the characteristic diffraction peaks of BiOBr can be well-indexed to the tetragonal phase whose lattice parameters are a = 3.915, c = 8.076 Å (space group: $P4/nmm$, JCPDS 73−2061). The different Ag content (1%, 3%, and 5%) of T−Ag composites were obtained after solvothermal treatment. The Ag characteristic peaks of T−1% Ag and T−3% Ag are not shown, attributing to the low-content of Ag. Regarding of T−5% Ag, the marked peaks (38.1 and 44.2°) can be perfectly indexed to (111) and (200) reflections of the face-centered cubic (fcc) phase of Ag (JCPDS 04−0783). Additionally, the shift of some BiOBr characteristic peaks (2θ = 25.26, 46.36 and 76.95°) and the reduction of BiOBr peaks (2θ = 25.26, 39.44, and 50.84°) are attributed to the Ag and Ti doping.[23] Moreover, the chemical elemental components of the samples are characterized by EDS spectrum, which indicates that the samples are composed of the elements Ag, Ti, O, Br, and Bi (see Figure S3 in the Supporting Information).

Although XRD andEDS result has effectively confirmed the existence of Ag element, it cannot distinguish its valence states. In order to investigate the Ag valence states, XPS spectra of 3% Ag/Ti-doped BiOBr was measured. The XPS spectra (see Figure S3 in the Supporting Information) of the as-prepared samples indicated the existence of Ag, Ti, Bi, O, and Br element, in accordance with the EDS and XRD results. And the XPS spectrum of Ag 3d (Figure 2d) indicate that there are two components after thermal reduction, attributed to Ag_2O (367.5 eV) and Ag^o (368.1 eV), respectively.[23,24] And the atomic rate of Ag/Bi and Ag^+/Ag^0 is 2.41/97.59 and 1.27/1, so the atomic rate of Ag doping content/Bi is about 1.38%. From the above discussion, it can be concluded that the surface states of Ag/Ti-doped BiOBr were multiple due to simultaneous doping and loading of Ag species. N_2 absorption analysis is carried to further characterize the porous structure of the as-prepared T−Ag samples (see Figure S4 in the Supporting Information), which show the adsorbed volume and pore volume of T−3% Ag are comparatively high. Furthermore, UV/vis diffuse reflectance spectra of the as-prepared samples show Ag decorating effectively increase the absorption under visible light (see Figure S5 in the Supporting Information). And the plasmon peak centered at around 500 nm of the Ag nanoparticles is not obvious because the content of loaded Ag is low.[25]

To explore the photocatalytic performance of the resultant samples for real applications, we investigated the photodegradation of dye molecules under daylight lamp illumination. Figure 3a shows the photolysis and degradation of RhB molecules by Ti-doped BrOBi, T−(1%, 3%, and 5%)Ag, C−Ag, and P−Ag as a function of irradiation time. The adsorption−desorption equilibrium for photocatalysts can be reached after stirring for 1 h under dark condition, and neither photolysis (without photocatalyst) nor catalysis (without light) exhibited degradation ability on RhB, suggesting that degradation ability is induced by photocatalysis. For comparison, Ag/Ti-doped BiOBr composites, which were obtained by three methods, could completely decompose RhB molecules. However, only about 50% is degraded by Ti-doped BrOBr after irradiation for 1 h. In addition, the effect of different Ag contents of T−Ag on their photocatalytic activity was investigated. As expected, all the T−Ag samples exhibit remarkable enhancement in photocatalytic activity in comparison with that of the Ti-doped BrOBr microspheres, which attribute to the improvement of photoabsorption and the charge separation.[26] Moreover, the photocatalytic activity of the T−Ag samples is highly dependent on Ag content. By contrast, the T−3% Ag sample displays the highest activity because of the optimal Ag decorated content for the charge separation and the higher adsorbed volume and pore volume.[27,28] The order of photocatalytic activity for the resultant samples can be summarized as follows: T−3% Ag ≥ C−Ag ≥ P−Ag > T−1% Ag > T−5% Ag > Ti-doped BrOBr. As observed, BiOBr with Ti doping and Ag decorating, which prepare by three methods, show almost the same activity. However, in comparison to chemical reduction and photoreduction, solvothermal approach is very simple and efficient. Besides efficiency, the durability is also indispensable to photocatalysts. As shown in Figure 3b, T−3% Ag photocatalysts are mechanically robust: they can be recovered and reused to catalyze five cycles of RhB degradation with inconspicuous decrease under direct reading lamp irradiation.

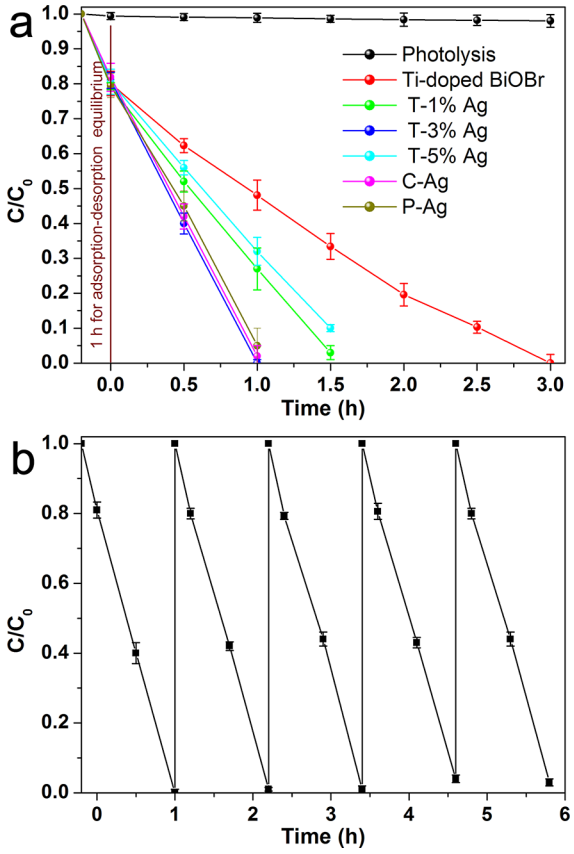

Figure 3. (a) Photocatalytic degradation of RhB over Ti-doped BiOBr, C−Ag, P−Ag, T−(1%, 3%, 5%)Ag samples, and (b) Cycling runs for the photodegradation of RhB over as-prepared T−3% Ag composites.

On the basis of our experiment results and reported literatures,[8a,14,29,30] the plausible reaction mechanism for the superior photocatalytic activity of T−Ag samples is proposed (Scheme 1). The daylight lamp irradiation activates T−Ag to generate strongly oxidative holes (h^+) in valence band and reductive electrons (e^-) in conduction band. In addition, the photogenerated electron−hole pairs are also formed on the surface of the loaded Ag due to the SPR. The electrons would transfer from the photoexcited Ag (Ag*) to the conduction band of Ti-doped BiOBr. Then these photoinduced electrons

dx.doi.org/10.1021/am301177k | ACS Appl. Mater. Interfaces 2012, 4, 4440−4444

Scheme 1. Schematic Illustration of the Photocatalytic Mechanism of RhB Degradation over T−Ag Photocatalyst

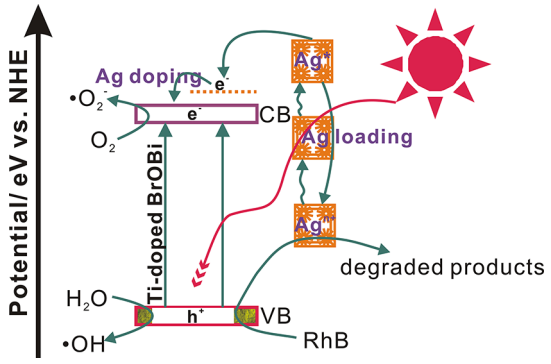

are trapped by molecular oxygen (O_2) to form superoxide ions ($\cdot O_2^-$). After the photogenerated electrons are released, Ag* would shift to more positive potentials to form positively charged Ag^{n+}, which was considered to be the active species. By oxidation of the RhB or accepting electrons from the conduction band of Ti-doped BiOBr, Ag^{n+} could return to Ag. The loaded and doped Ag acts as the electron receptor, which inhibits the recombination of photogenerated electrons and holes. Moreover, the photoinduced holes (h_{VB}^+) can oxidize RhB directly or react with H_2O to generate active radical species (•OH) and H^+, and H^+ subsequently react with the absorbed O_2 to yield •OH. These oxidative species will also result in the degradation of RhB molecules.

$$\text{Ag/Ti-doped BiOBr} + \text{visible light} \rightarrow h_{VB}^+ + e_{CB}^-$$

$$e_{CB}^- + O_2 \rightarrow \cdot O_2^-$$

$$h_{VB}^+ + H_2O \rightarrow \cdot OH + H^+$$

$$O_2 + 2H^+ + 3e_{CB}^- \rightarrow \cdot OH + OH^-$$

$$\cdot OH \text{ or } h_{VB}^+ \text{or } Ag^{n+} + \text{RhB} \rightarrow \text{degraded products}$$

In summary, for the first time, the highly active visible-light-induced BiOBr photocatalysts with Ti doping and Ag decorating has been prepared by solvothermal method. The photocatalytic activity of the T−Ag samples is highly dependent on Ag content and the T−3% Ag photocatalyst exhibits highest activity and excellent durability for the degradation of RhB due to the optimal Ag content. The enhanced photocatalytic activity was attributed to the improvement of photoadsorption and the charge separation. This may pave the way for practical applications of Ag decorated Ti-doped BiOBr photocatalyst under sunlight.

■ ASSOCIATED CONTENT

Ⓢ Supporting Information

Experimental section, FE-SEM and TEM images, XPS and EDS spectra, N_2 adsorption−desorption, and UV/vis diffuse reflectance spectra. This material is available free of charge via the Internet at http://pubs.acs.org/.

■ AUTHOR INFORMATION

Corresponding Author

*E-mail: polymer_jiang@hotmail.com.

Notes

The authors declare no competing financial interest.

■ ACKNOWLEDGMENTS

This work was financially supported by the Qianjiang Talents Project of Zhejiang Province (2010R10023), the Scientific Research Foundation for the Returned Overseas Chinese Scholars, the State Education Ministry (1001603-C), the Natural Science Foundation of Zhejiang Province (Y4100045), Training Foundation for the Excellent Young Talents by the Key Laboratory of Advanced Textile Materials and Manufacturing Technology (ATMT), Ministry of Education (2011QN04), and the National Natural Science Foundation of China (51133006).

■ REFERENCES

(1) Feng, Y.; Li, L.; Li, J.; Wang, J.; Liu, L. *J. Hazard. Mater.* **2011**, *192*, 538−544.
(2) Ai, Z.; Ho, W.; Lee, S.; Zhang, L. *Environ. Sci. Technol.* **2009**, *43*, 4143−4150.
(3) Fang, Y.; Huang, Y.; Yang, J.; Wang, P.; Cheng, G. *Environ. Sci. Technol.* **2011**, *45*, 1593−1600.
(4) Xu, J.; Meng, W.; Zhang, Y.; Li, L.; Guo, C. *Appl. Catal., B* **2011**, *107*, 355−362.
(5) Zhang, X.; Ai, Z.; Jia, F.; Zhang, L. *J. Phys. Chem. C* **2008**, *112*, 747−753.
(6) Shan, Z.; Wang, W.; Lin, X.; Ding, H.; Huang, F. *J. Solid State Chem.* **2008**, *181*, 1361−1366.
(7) (a) Cheng, H.; Huang, B.; Wang, Z.; Qin, X.; Zhang, X.; Dai, Y. *Chem.—Eur. J.* **2011**, *17*, 8039−8043. (b) Zhang, J.; Zhu, H.; Zheng, S.; Pan, F.; Wang, T. *ACS Appl. Mater. Interfaces* **2009**, *1*, 2111−2114. (c) Zhu, P.; A. Sreekumaram, N.; Peng, S.; Yang, S.; Seeram, R. *ACS Appl. Mater. Interfaces* **2012**, *4*, 581−585. (d) Jiang, G.; Wang, R.; Jin, H.; Wang, Y.; Sun, X.; Wang, S.; Wang, T. *Powder Technol.* **2011**, *212*, 284−288.
(8) (a) Wang, R.; Jiang, G.; Ding, Y.; Wang, Y.; Sun, X.; Wang, X.; Chen, W. *ACS Appl. Mater. Interfaces* **2011**, *3*, 4154−4158. (b) Wang, R.; Wang, X.; Xi, X.; Hu, R.; Jiang, G. *Adv. Mater. Sci. Eng.* **2012**, 409379. (c) Iizuka, K.; Wato, T.; Miseki, Y.; Saito, K.; Kudo, A. *J. Am. Chem. Soc.* **2011**, *133*, 20863−20868. (d) Zhang, Y.; Yuan, X.; Wang, Y.; Chen, Y. *J. Mater. Chem.* **2012**, *22*, 7245−7251.
(9) Jiang, G.; Zheng, X.; Wang, Y.; Li, T.; Sun, X. *Powder Technol.* **2011**, *207*, 465−469.
(10) Jia, Z.; Wang, F.; Xin, F.; Zhang, B. *Ind. Eng. Chem. Res.* **2011**, *50*, 6688−6694.
(11) Seh, Z. W.; Liu, S.; Low, M.; Zhang, S.; Liu, Z.; Mlayah, A.; Han, M. *Adv. Mater.* **2012**, *24*, 2310−2314.
(12) Wang, P.; Huang, B.; Qin, X.; Zhang, X.; Dai, Y.; Wei, J.; Whangbo, M. *Angew. Chem., Int. Ed.* **2008**, *47*, 7931−7933.
(13) Ma, R.; Sasaki, T.; Bando, Y. *J. Am. Chem. Soc.* **2004**, *126*, 10382−10388.
(14) Cheng, H.; Huang, B.; Wang, P.; Wang, Z.; Lou, Z.; Wang, J.; Qin, X.; Zhang, X.; Dai, Y. *Chem. Commun.* **2011**, *47*, 7054−7056.
(15) Liu, J.; Sun, Y.; Li, Z. *Cryst. Eng. Comm.* **2012**, *14*, 1473−1478.
(16) Xi, G.; Ye, J.; Ma, Q.; Su, N.; Bai, H.; Wang, C. *J. Am. Chem. Soc.* **2012**, *134*, 6508−6511.
(17) Matsubara, K.; Tatsuma, T. *Adv. Mater.* **2007**, *19*, 2802−2806.
(18) Wang, Z.; Liu, J.; Chen, W. *Dalton Trans.* **2012**, *41*, 4866−4870.
(19) Jana, S.; Pande, S.; Sinha, A. K.; Sarkar, S.; Pradhan, M.; Basu, M.; Saha, S.; Pal, T. *J. Phys. Chem. C* **2009**, *113*, 1386−1392.
(20) Zhang, H.; Liang, C.; Liu, J.; Tian, Z.; Wang, G.; Cai, W. *Langmuir* **2012**, *28*, 3938−3944.
(21) Georgescu, D.; Roiban, L.; Ersen, O.; Ihiawakrim, D.; Baia, L.; Simon, S. *RSC Adv.* **2012**, *2*, 5358−5369.
(22) Wang, R.; Jiang, G.; Wang, X.; Hu, R.; Xi, X.; Bao, S.; Zhou, Y.; Tong, T.; Wang, S.; Wang, T.; Chen, W. *Powder Technol.* **2012**, *228*, 258−263.
(23) Xin, B.; Jing, L.; Ren, Z.; Wang, B.; Fu, H. *J. Phys. Chem. B* **2005**, *109*, 2805−2809.

(24) Thomas, M. A.; Sun, W. W.; Cui, J. B. *J. Phys. Chem. C* **2012**, *116*, 6383−6391.
(25) Ren, J.; Wang, W.; Sun, S.; Zhang, L.; Chang, J. *Appl. Catal., B* **2009**, *92*, 50−55.
(26) Wang, D.; Xue, G.; Zhen, Y.; Fu, F.; Li, D. *J. Mater. Chem.* **2012**, *22*, 4751−4758.
(27) Kang, S. W.; Char, K.; Kang, Y. S. *Chem. Mater.* **2008**, *20*, 1308−1311.
(28) Yu, J.; Liu, W.; Yu, H. *Cryst. Growth Des.* **2008**, *8*, 930−934.
(29) Gondal, M.; Chang, X.; Ali, M.; Yamani, A.; Zhou, Q.; Ji, G. *Appl. Catal. A: Gen.* **2011**, *397*, 192−200.
(30) Ma, J.; Tai, G.; Guo, W. *Ultrason. Sonochem.* **2010**, *17*, 534−540.